U.S. DEPARTMENT OF COMMERCE
National Oceanic and Atmospheric Administration
Environmental Research Laboratories

NOAA Technical Memorandum ERL NSSL-67

RADAR RAINFALL PATTERN OPTIMIZING TECHNIQUE

Edward A. Brandes

National Severe Storms Laboratory
Norman, Oklahoma
March 1974

TABLE OF CONTENTS

LIST OF FIGURES

LIST OF TABLES

RADAR RAINFALL PATTERN OPTIMIZING TECHNIQUE

by

Edward A. Brandes

Estimates of precipitation are improved when quantitative radar data are combined with rain gage observations. Gage observations are used to calibrate radar data as well as to estimate precipitation in areas without radar data.

Error estimates of areal precipitation depth for five cases of widespread rainfalls over a 1000 n mile^2 watershed, averaged 8 and 15 percent with densities of one gage per 270 and 675 n miles^2, respectively. Precipitation estimates derived from an objective analysis of rainfall depths observed at the calibrating gages alone produced errors of 10 and 21 percent. Radar data added to gage observations increased the explained variance at test gages, beyond that given by gage data alone, from 66 to 72 percent and 50 to 59 percent for the same calibrating gages.

Large storm-to-storm variations in average radar calibration and large spatial correction variations within storms were attributed to propagation effects.

1. INTRODUCTION

Hydrologic applications of radar data should increase with more timely availability of processed digital radar data. The accuracy of radar measured rainfall has been discussed by many authors. Joss et al. (1968), Woodley and Herndon (1970), Huff (1967), and Wilson (1970a) represent recent applications. Practical considerations of radar rainfall measurements, with a description of the NSSL WSR-57 data collection system, are in Wilk and Kessler (1970). Although radar measures precipitation variability accurately, calibration against in-situ measurements is highly desirable (Hitchfield and Bordan, 1954).

Wilson (1970a) has shown that radar derived precipitation estimates when calibrated with gage densities as little as one gage/1000 n miles^2, are more accurate than estimates taken from gages alone with spacing one/250 n miles^2. In Wilson's study, a single calibration factor (the sum of observed rainfalls at calibrating gages divided by the sum of the uncorrected radar estimates) was uniformly applied to the radar data. However, preliminary investigations here as well as the work of others, have revealed that large spatial variations in calibrations are likely. This study attempts to improve radar estimates by generating a matrix of calibration factors that reflect these variations. This research aims to develop tools for combining radar and rain gage data under operational conditions to produce timely and accurate precipitation maps.

2. OUTLINE OF PROGRAM LOGIC

This section describes the various radar and rain gage data handling procedures for producing radar precipitation estimates. A flow diagram is given in figure 1. Rainfall totals are accumulated in polar format after converting radar reflectivities to rainfall rates. The uncalibrated radar data are transformed to Cartesian coordinates at a storms' end. Rain gage observations are then introduced to calibrate the radar and generate precipitation estimates in areas where quality radar data are unavailable. Illustrations of the various precipitation fields at grid points near a calibrating rain gage are presented.

2.1 Radar Field - Uncalibrated

To convert radar reflectivities into rainfall depths we begin with the radar equation in the form

$$\overline{P_r} = 3.88(10^{-26})P_t h G^2 \phi\theta |K|^2 Z_e / \lambda^2 r^2 , \qquad (1)$$

where the variables are as shown in table 1 (Probert-Jones, 1962) and the radar has a logarithmic response.

By converting $\overline{P_r}$, the average power received in watts, to $\overline{P_r}$ dBm, normalizing to 120 n miles, and after correcting for the difference between $\overline{\log P_r}$ and $\log \overline{P_r}$ (approximately 2.5 dB), we can write (1) in logarithmic form as

$$\log Z_e = 0.1 P_r + 12.13. \qquad (2)$$

Corrections have not been applied for atmospheric absorption or radar signal attenuation. The error in signal processing (integration) for the NSSL WSR-57 is $\pm$ 1 dB. For routine operation, the overall radar and signal generator instability is estimated to be $\pm$ 3 dB.

Rainfall rates (R) in mm/hr are estimated with the Marshall-Palmer relationship

$$Z_e = 200R^{1.6}. \qquad (3)$$

However, the described methodology minimizes the impact of the particular Z-R relationship because the rain

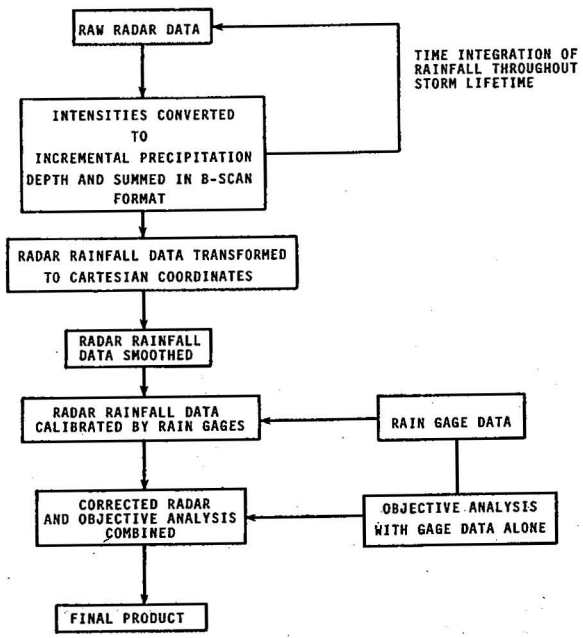

Figure 1. Program flow diagram.

Table 1. Summary of Radar Equation Terms and Characteristics of the NSSL WSR-57 Radar

$\overline{P}_r$	Average power received (w)	
P_t	Peak transmitted power (w)	$2.96(10)^5$
h	Pulse length (m)	1200
G^2	Antenna gain squared	$4.169(10)^7$
ϕ	Vertical beam width (°)	2
θ	Horizontal beam width (°)	2
$\|K\|^2$	Dielectric factor	0.93
Z_e	Equivalent reflectivity factor (mm^6/m^{-3})	
r	Range (n miles)	
λ	Wavelength (cm)	10.55
$3.88(10)^{-26}$	Constant and units conversion	

gage values are used to adjust the raw radar field.

Incremental depth accumulations are summed from raw data in azimuthal sections 2 degrees wide and 1 n mile (1.85 km) long. The calculated rates are multiplied by the time difference between observations, usually 5 min in the test data. Tilt data are not considered here. The digital radar data are presented by the computer printer in B-scope format, i.e., with azimuth and range as Cartesian coordinates (fig. 2). Conversion from B-scan to a conformal display (fig. 3) takes place at a storms' end, or when additional accumulations are likely to be small. The selected grid spacing of 1.25 n miles (2.32 km) corresponds closely with the resolution of the radar. Consequently, only small errors are introduced in the scan conversion used in this experiment.

2.2 Smoothing the Uncalibrated Radar Field

The rainfall field defined by the radar data alone is smoothed by a light filtering operation to reduce small-scale radar fluctuations (fig. 4). Smoothed grid values of radar rainfall, $A_S(I,J)$, are determined from the nine-point operator

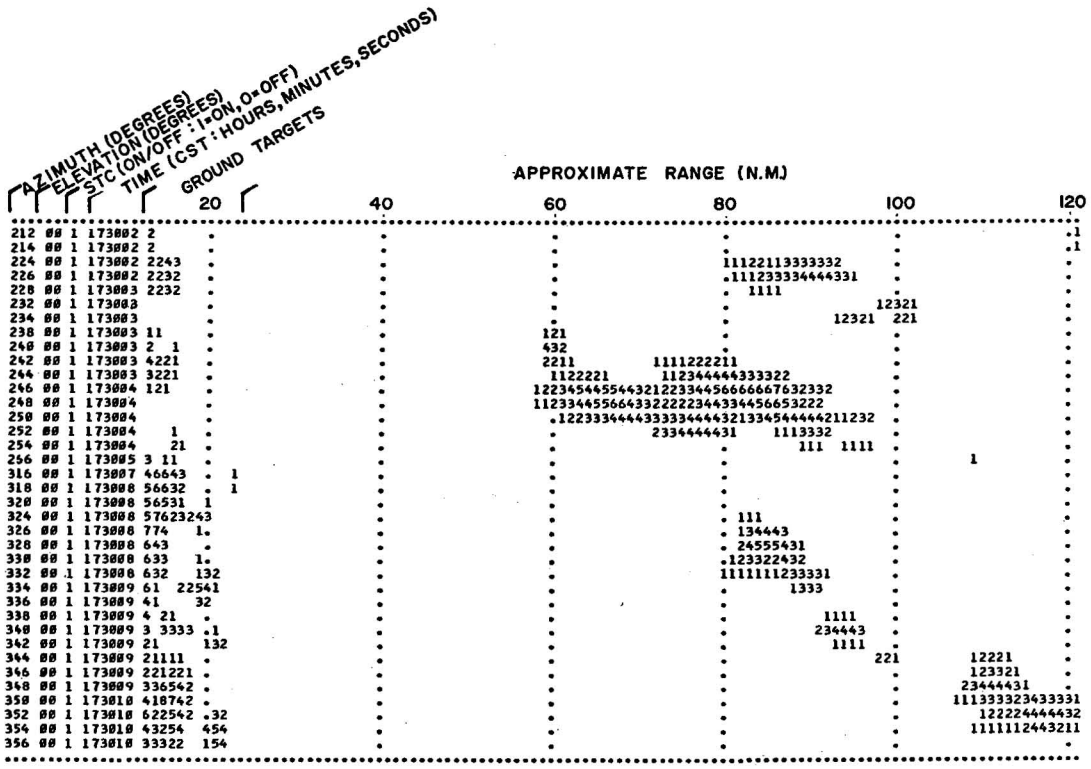

Figure 2. B-scope (azimuth-range) presentation of digital radar echoes in special printer format. Only azimuths with precipitation data beyond 20 n miles are printed, zeroes (no echo) are suppressed, and range marks are added to aid interpretation.

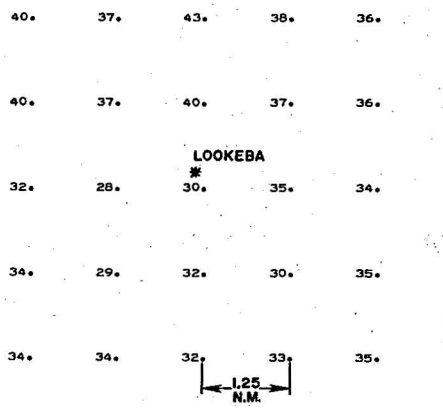

Figure 3. Estimated precipitation depth (raw radar) in hundredths of inches. Observed depth at Lookeba, Okla., 157.

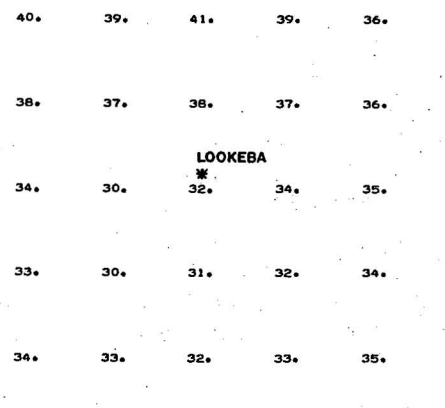

Figure 4. Smoothed radar field.

$$A_s(I,J) = A(I,J)+\frac{a}{2}(1-a)[A(I,J+1)+A(I,J-1)+A(I+1,J)+A(I-1,J)-4A(I,J)] + \frac{a^2}{4}[A(I+1,J+1)+A(I+1,J-1)+A(I-1,J+1)+A(I-1,J-1)-4A(I,J)], \quad (4)$$

where (a) is equal to 1/2. Shuman (1957) has used this simple filter in meteorological numerical analysis to suppress short wavelengths. Wavelengths of four grid lengths are smoothed to 50 percent of their original amplitude, while wavelengths longer than 12 grid lengths are essentially unchanged.

2.3 Calibrating the Radar Field

The smoothed radar field is then calibrated by rain gages. Multiplicative (calibration) factors are determined at each rain gage site that records 0.10 inch or more of precipitation. (Gages recording less than 0.10 inches are not used because small differences between observed amounts and uncalibrated radar data can lead to spuriously large calibration factors.) Factors are determined by averaging the raw radar data within 25 km^2 of the gage (all data points that fall within 2.8 km of the gage site) and then dividing this into the gage amount. Wilson (1970b) discusses the effects of areal averaging and observation frequency on rainfall estimate error.

Barnes' (1964) objective analysis scheme is used to move the correction factors at rain gage sites onto the field of grid points. The weight (WT_i) each gage calibration (G_i) receives at a particular grid point is given by

$$WT_i = \exp(-r^2/EP) \quad (5)$$

where r is the distance between the gage and grid point in kilometers. EP controls the degree of smoothing and is determined partly by the average rain gage spacing. Operationally, EP is kept as small as possible to preserve detail in the input observations. When EP equals 600 km^2, about 25 percent of the amplitude of a 60 km wavelength is retained. This increases to approximately 60 percent when EP equals 200 km^2.

Two passes are made through the data. On the first pass, the first-guess grid point calibrations (F_1) are computed as

$$F_1 = \sum_{i=1}^{N} WT_i G_i / \sum_{i=1}^{N} WT_i. \quad (6)$$

N is the number of gages. (In practice, gages with very small weights - exponent arguments less than -12 - are not summed.) The difference (D_i) is calculated at each gage location from

$$D_i = G_i - F_1 \ , \qquad (7)$$

where the first-guess estimate (F_1) is taken at the grid point nearest the rain gage rather than at the gage itself.[1]

The second pass uses (5) with EP reduced by 1/2 and analyzes the difference field by the same method. Difference values calculated at each grid point are added to the first-guess field. Thus, the final grid point calibration (fig. 5), generally determined from calibration data of more than one calibrating gage, is given by

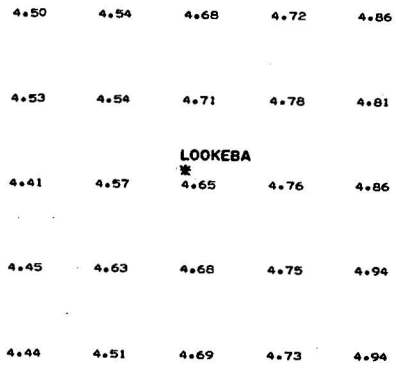

Figure 5. Radar calibration field. The difference between the actual value at Lookeba (4.76) and the surrounding grid point values results from the influence of other nearby gage calibrations.

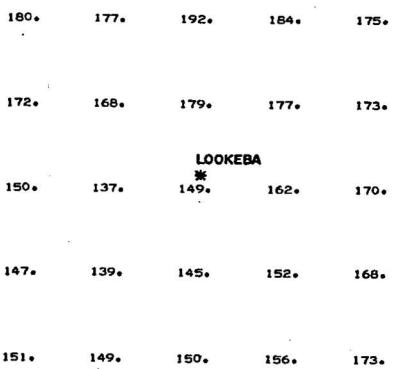

Figure 6. Corrected (calibrated) precipitation field.

$$F_2 = F_1 + \sum_{i=1}^{N} WT_i D_i \Big/ \sum_{i=1}^{N} WT_i \ . \qquad (8)$$

Multiplication of the calibration field with the lightly smoothed radar field gives the corrected (calibrated radar precipitation field (fig. 6). Further details of the technique, only briefly outlined here, can be found in Barnes (1973).

2.4 Gage Derived Precipitation Field

A second objective analysis of the precipitation field is made from all available rain gage data, including previously omitted gages that recorded less than 0.10 inch and gages within the radar ground pattern (see fig. 7). This second precipitation estimate in the radar data areas is also the only estimate in radar ground clutter area and at excessive distances from the radar, as well as areas where radar data are incomplete due to power failures, or where anomalous propagation (AP) obscures precipitation echoes. The procedure is similar to that already

---

1 This approximation introduces negligible error since in our study the maximum distance from a rain gage to the nearest grid point never exceeds 1.2 km. For applications with larger grid spacings, F_1 should be calculated by interpolation to the gage from the surrounding grid points.

outlined.[2] A smaller EP value is selected because of the increased density of observations.

The gage-derived precipitation field also is used for further calibration in the vicinity of the input gages (see below). Because EP is reduced to suppress the weights of distant gages and because the calibrations for the gage-calibrated radar data were averaged about the gage sites, this field is more exacting at the gage sites than the corrected radar field.

2.5 Final Analysis - Gage Derived and Calibrated Radar Precipitation Fields Combined

Finally the corrected radar and gage estimated rainfall fields are combined (fig. 8). At grid points coinciding with a gage location, a 100 percent weight is given to the gage estimated field. The weight decreases linearly to 0 percent, and the radar field weight increases to 100 percent as the distance from the nearest calibrating gage increases to 11 km. This figure (11 km) is chosen to restrain the gage influence beyond a distance corresponding to the dimension that characterizes most of the small-scale precipitation variance. Qualitatively, a slight further smoothing of wavelengths less than 22 km occurs near a calibrating gage. By having small regions of influence, we insure a close fit at the gage sites and the radar observed precipitation detail between gages is retained. Ideally, this distance could be a function of a measured scale parameter based on the radar data or the variance of the input rain gage depths.

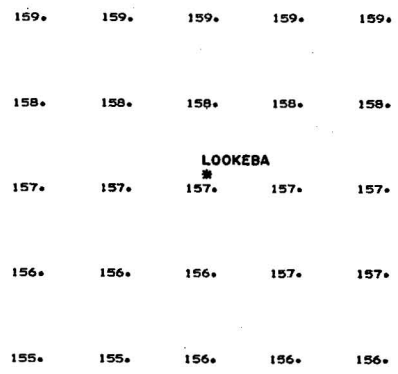

Figure 7. Precipitation field derived from gage data alone.

At grid points farther than 11 km from a calibrating gage, the calibrated radar field is used exclusively. Areas where only one field indicates precipitation, that field is considered to estimate the true precipitation.

Contoured maps (figs. 9 and 10) illustrate gage-derived and combined precipitation fields. The combined

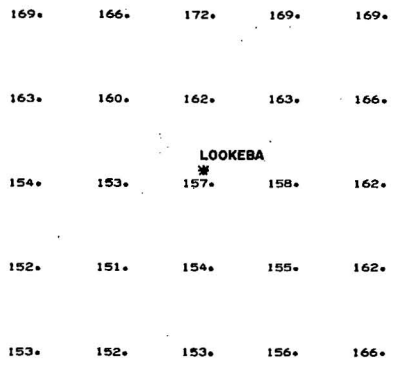

Figure 8. Final analysis.

---

2 An application of the Cressman (1959) analysis method to rain gage data is described by Maine and Gauntlett (1968).

precipitation field reveals that induced precipitation gradients are likely at boundaries separating fields derived exclusively from calibrated radar or rain gage data (e.g., the radar ground pattern edge). Because of the relatively wide spacing between rain gages, the rain gage field characterically indicates larger elements than are contained in the actual precipitation and radar fields.

3. APPLICATION AND EVALUATION

Six convective precipitation events, lasting from 4 to 16 hours were selected for study. The chosen analysis area was 90 x 90 n miles with a grid spacing of 1.25 n miles. Radar data within the analysis region were calibrated with climatological rain gage observations having densities of one gage per 270 and 675 n miles^2, i.e., 30 and 12 gages (fig. 11). Average

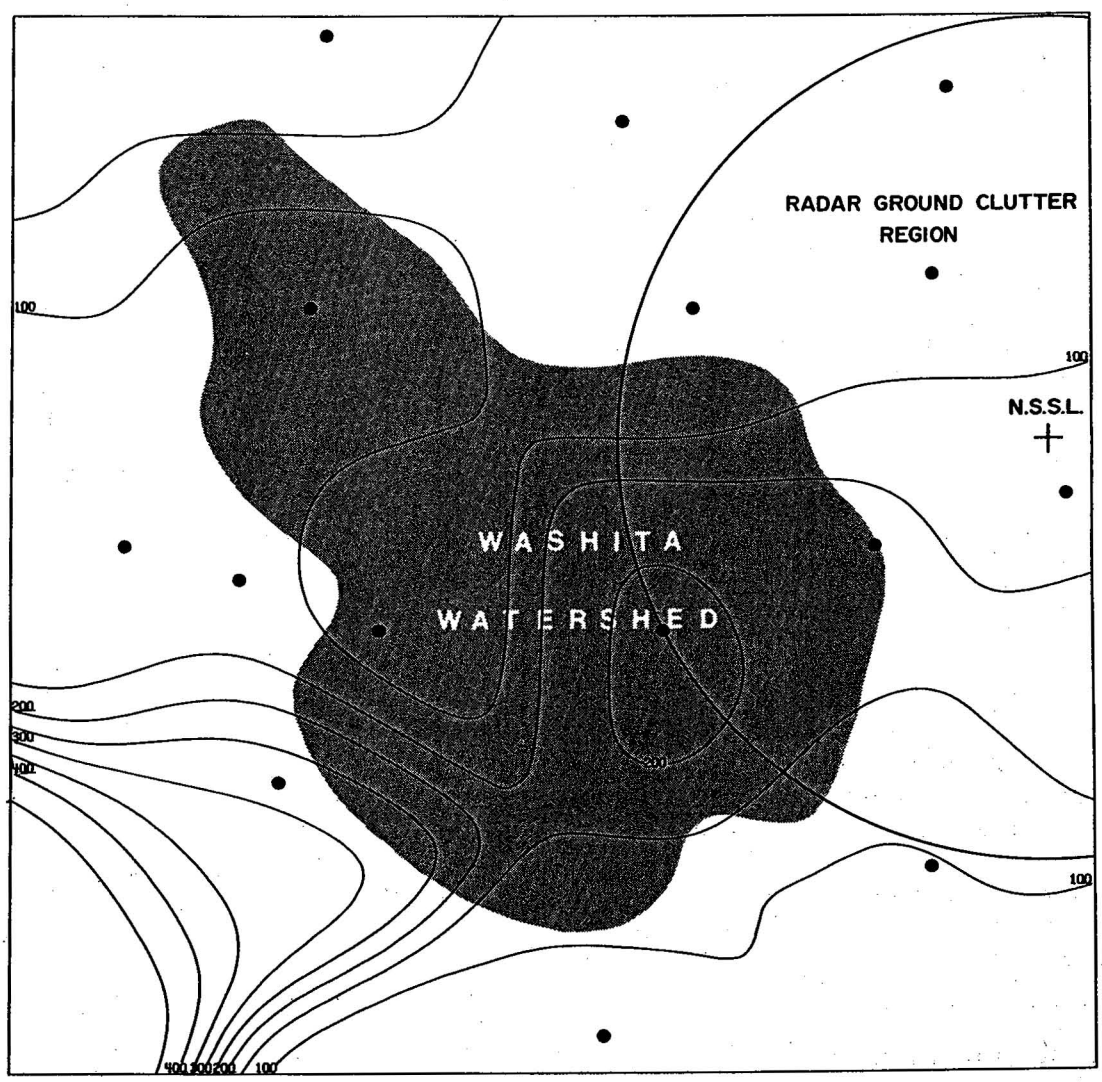

Figure 9. Gage derived precipitation field for 26-27 April 1972. Dots are rain gage locations. Depths are in hundredths of inches.

precipitation depths then were computed for the Washita Watershed, a 1000 n miles^2 subsection of the analysis grid and located just west of NSSL. Approximately 20 percent of this area is within the radar ground pattern. Actual average depths of rainfall in the watershed were calculated from 158 uniformly spaced rain gages operated by the Agriculture Research Service (ARS), U. S. Department of Agriculture. Two aspects of the program's accuracy--how well the average watershed precipitation was estimated and how well the spatial variance within the watershed was described--are now considered.

Average watershed precipitation depth estimates at steps in the program logic are given in table 2. The significant underestimate with raw radar data and the storm-to-storm variations between actual rainfall and radar depths reveal the need for calibration. Furthermore, large spatial variations in calibration factors (not reproduced here) suggest the desirability of a calibration scheme that considers these variations.

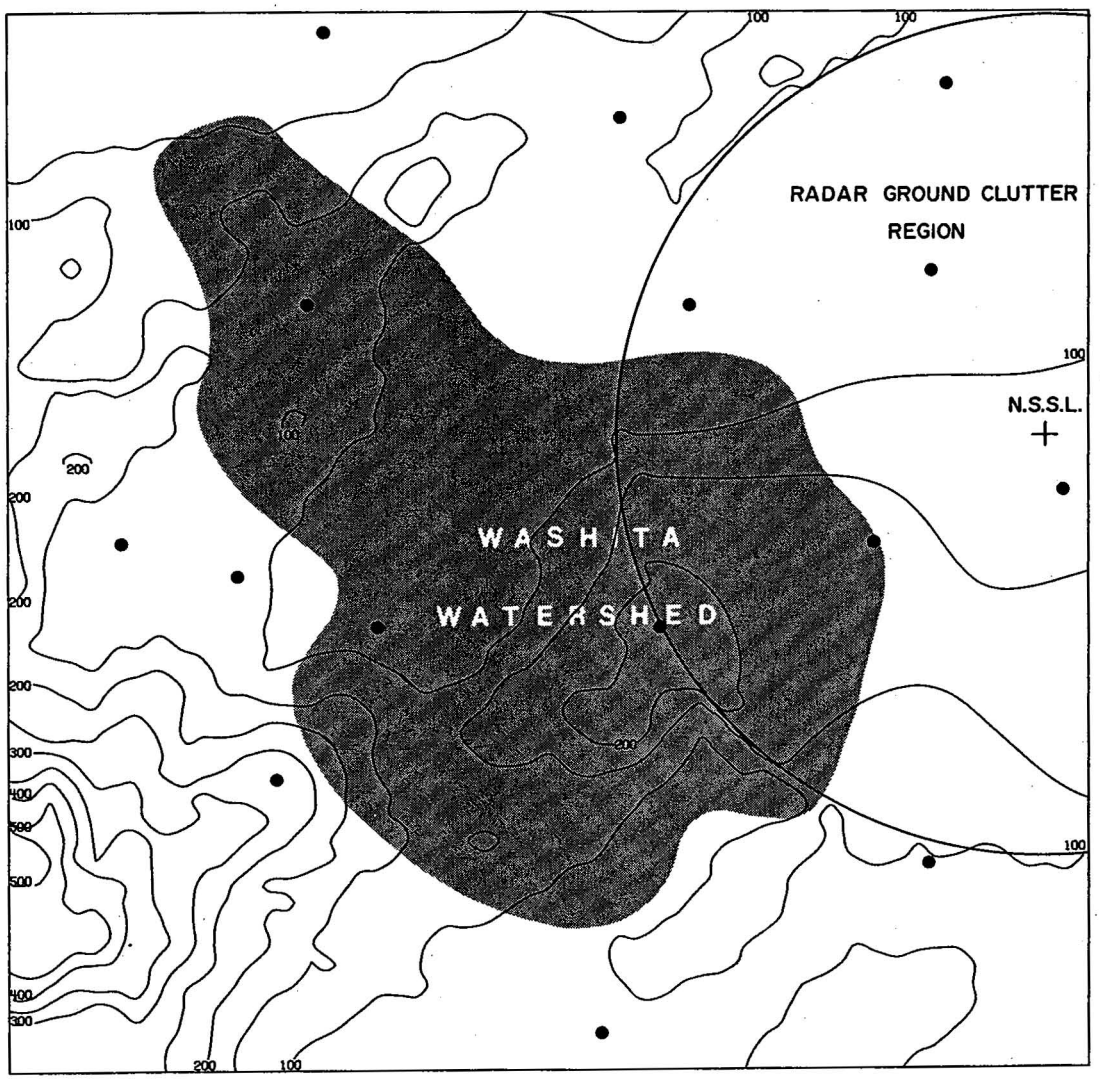

Figure 10. Final precipitation analysis (calibrated radar and gage derived fields combined).

Table 2. Comparison of Actual Watershed Precipitation with Program Depth Estimates

	STORM						AVERAGE ERROR[c]
	A	B	C	D	E	F	(%)
PRECIPITATION ESTIMATES WITH CALIBRATED RADAR[a]							
Watershed Depth	0.70	1.28	0.82	1.53	1.20	0.07	
Raw Radar	0.42	0.84	0.33	0.25	0.57	0.05	
Ratio (watershed/radar)	1.7	1.5	2.5	6.1	2.1	1.4	
Calibrated Radar[d]							
270 n miles^2/gage	0.64	1.07	0.87	1.65	1.22	0.06	8
675 n miles^2/gage	0.71	0.97	1.06	1.22	1.17	0.06	16
PRECIPITATION ESTIMATES WITH INPUT GAGE OBSERVATIONS[b]							
Watershed Depth	0.75	1.24	0.75	1.58	1.14	0.06	
Input Gage Estimate[e]							
270 n miles^2/gage	0.76	1.38	0.95	1.66	1.21	0.06	10
675 n miles^2/gage	0.60	1.53	1.12	1.64	1.07	0.26	21
COMBINED (FINAL) PROGRAM ESTIMATE[b]							
Watershed Depth	0.75	1.24	0.75	1.58	1.14	0.06	
Final Analysis							
270 n miles^2/gage	0.72	1.23	0.86	1.76	1.23	0.07	8
675 n miles^2/gage	0.70	1.06	1.04	1.39	1.19	0.24	15

[a] Excludes that portion of the watershed within the radar ground pattern (actual depth computed from 130 ARS gages).

[b] Entire watershed (actual depth computed from 158 ARS gages).

[c] Excludes Storm F in which spotty precipitation was observed.

[d] EP values of 600 and 800 km^2 were selected for determining the calibration fields.

[e] EP values of 200 and 600 km^2 were used to compute the gage derived precipitation field.

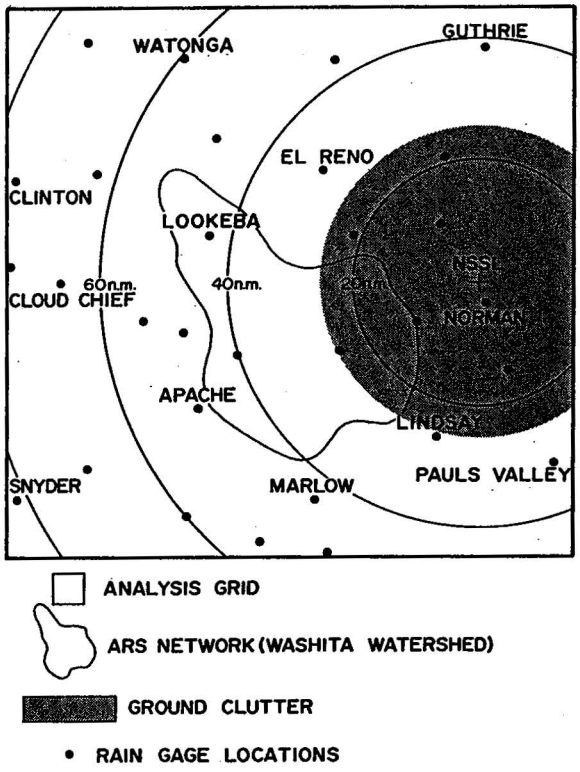

Figure 11. Analysis region. Showing gage and watershed locations. Labeled gages have 675 n miles^2/gage spacing.

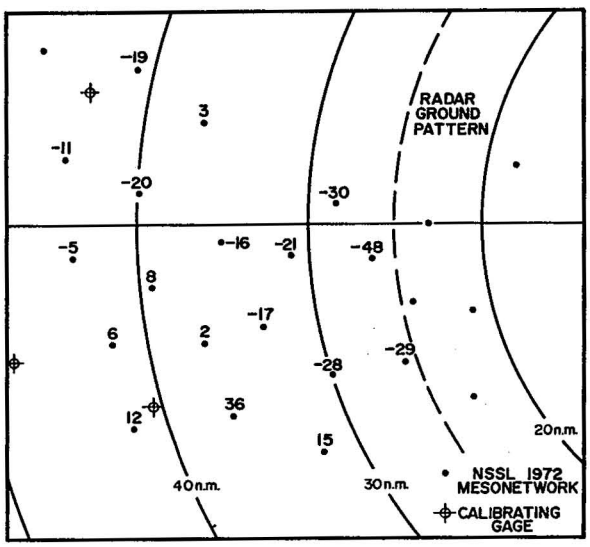

Figure 12. Average error (hundredths of inches) at test gage sites. Observed minus estimated depth. Calibration density - 270 n miles^2/gage.

The average errors in the final analysis depth estimates (8 and 15 percent) are less than the errors made from gage observations alone (10 and 21 percent). Although the value of radar in this small storm sample may be less than desirable, radar is, of course, valuable for detecting areas of precipitation and directing the operator's attention to certain areas where high accumulations of rainfall are likely.

Table 3 shows that the relative dispersion of precipitation (standard deviation times 100 percent divided by the mean) in the final analysis is lower than the actual dispersion found with the dense network of ARS gages. Wilson (1971) and Huff (1967) noted that usually dense gage data have only slightly larger dispersions than that observed by radar. Herein the additional smoothing originates in the gage-derived precipitation field which fills the ground clutter area and from the combination routine at the calibration gages.

Point precipitation estimates were produced at several test locations interspaced among the calibration gages; with both the calibrated radar precipitation field (before combining with the gage-derived field) and the climatological gage-derived precipitation field (table 4). Radar derived point rainfall estimates are subject to a variety of errors that include sampling volume differences, radar beam elevation, spatial variations in the Z-R relationship, and propagation effects.

Because radar derived estimates use gage data for their calibration and draw upon the radar observations between gages, their higher correlations with corrected radar data are expected. The added value of radar in this storm sample is indicated by the increases in explained variance from 66 to 72 percent and from 50 to 59 percent with different gage densities.

Errors in the calibrated radar and rain gage fields differ in origin. Errors in analyzing widely spaced gage data arise because the distance between gages is larger than the precipitation element scale. Systematic errors were found to remain in the radar precipitation field, in between calibration gages, after the calibration factors are applied.

The average error field (at the test sites) for the six storms (fig. 12) shows that large overestimates occurred at all test gages within 55 km (30 n miles) of the radar. At larger distances, in the west-southwest, the error field is characterized by large underestimates at test gages and generally small overestimates in the west-northwest.

Because the basic error field was repetitive, the six cases studied had similar storm locations, and there was no reason to suspect program bias, we concluded that these errors, beyond the normal ground pattern which remain after calibration, and the spatial variation in gage calibrations, may have resulted from propagation effects. Battan (1959) has described a condition of "thunderstorm superrefraction" in which local temperature inversions and specific humidity variations can produce strong ducting near thunderstorms. For fair weather conditions, the ground clutter was wholly within the 46 km (25 n miles) limit within which radar data were not used in this study. It may be, however, that ground targets beyond 46 km, not obvious before and after rainfall, are enhanced by ducting while it rains.

Ground targets close to the radar may block or distort the radar beam. Therefore, at all ranges precipitation measurements would be with less than the full beam width and perhaps restricted to the beam's upper portion. Strong vertical reflectivity gradients often observed near the ground (e.g., the data of Chmela, 1958, or Aoyagi, 1972) in thunderstorms could produce large over or underestimates of precipitation.

If the repetitive nature of the error fields is supported in additional tests, the development of local empirical correction factors might be important; it may then be desirable to place calibrating gages in known problem areas.

Table 3. Comparison of Actual and Estimated Precipitation Relative Dispersion (percent)

	STORM					
	A	B	C	D	E	F
Actual (158 ARS gages)	45	51	59	16	39	270
Combined Analysis (final)						
270 n miles^2/gage	42	36	39	22	29	216
675 n miles^2/gage	38	33	46	29	29	117

Table 4. Correlation Coefficient Between Estimated and Observed Rainfall Depths at Test Gages Not Used for Calibration (100 Cases)

	GAGE DENSITY[a]	
	1 Gage/270 n miles^2	1 Gage/675 n miles^2
Calibrated Radar Estimate	0.85 (72)[b]	0.77 (59)
Estimate from Input Gage Amounts	0.81 (66)	0.71 (50)

a The average distance between input gages is 7 and 13 n miles

b Explained variance in percent

Finally, watershed precipitation was estimated with the Marshal Palmer Z-R relationship by varying the radar calibration figures and with the Miami relationship ($Z_e = 300R^{1.4}$) used by Gerrish and Hiser (1965) for Florida thunderstorms. Note that calculated total storm depths (see table 5) are practically the same in the three examples given, which indicates that errors in the radar hardware calibration and the particular Z-R relationship selected become minor when the radar is adjusted by rain gage observations.

4. SUMMARY

A logical procedure has been developed for combining radar data with rain gage observations to improve precipitation estimates. Besides calibrating the radar, gage observations provide precipitation estimates in areas without quality radar data (e.g., ground clutter regions, at excessive distances from the radar, and in areas where there is AP). For a small sample of test cases, a radar-rain gage combination reduced the average error in precipitation estimates made only using the gages from 10 to 8 percent and from 21 to 15 percent for gage densities of one gage per 270 and 675 n miles^2, respectively.

The addition of radar data increased the explained variance at test gages, above that by gage observations alone, from 66 to 72 percent and 50 to 59 percent for densities of one gage per 270 and 675 n miles^2.

Small-scale repetitive errors in precipitation estimates were found in the radar field after calibrating the radar with the above gage densities. These errors and the spatial variation among calibration factors appear to result from propagation effects. The small-scale recurring errors limit radar data to use in watersheds of less than a few hundred square miles; unless a calibrating gage exists within the watershed or additional local corrections are applied. These errors become less important the larger the area over which the depths are averaged.

Table 5. Effect of Daily Radar System Calibration and Selection of Z-R Relationship on Total Storm Depth (26-27 April 1972)

Digital Class Interval[b]	Actual Calibration	Calibration of 14-15 April	Miami Z-R Relationship with Actual Calibration
	Assigned Precipitation Rate (Inches/Hour)		
1	0.03	0.10	0.03
2	0.07	0.19	0.06
3	0.15	0.39	0.15
4	0.33	0.91	0.36
5	0.68	1.88	0.83
6	1.39	3.35	1.73
7	3.20	7.17	4.28
8	6.77	17.51	10.58
9	12.94	38.64	26.14
	Calibrated Radar Estimate[a] (Inches)		
	1.07	1.05	1.06
	Final Program Estimate (Inches)		
	1.23	1.22	1.22

[a] For that fraction of the network within the radar umbrella.

[b] The highest class interval recorded in the area of radar coverage was 7.

Radar calibration variations, thought by some to be spatial and temporal changes in the Z-R relationship, may be at least partially caused by propagation effects.

5. REFERENCES

Aoyagi, J., 1972: Cloud top height measurements by radar, Preprints of papers, 15th Radar Meteor. Conf., Champaign, Ill., Amer. Meteor. Soc., 132-135.

Barnes, S. L., 1964: A technique for maximizing details in numerical weather map analysis, J. Appl. Meteor., 3, No. 4, 396-409.

Barnes, S. L., 1973: Mesoscale objective map analysis using weighted time-series observations, NOAA Tech Memo ERL NSSL-62, Norman, Oklahoma, 60 pp.

Battan, L. J., 1959: Radar Meteorology. The University of Chicago Press.

Chmela, A. C., 1958: Reflectivity measurements in the vertical through a severe squall line. Proceedings 7th Weather Radar Conf., Miami, Fla., Amer. Meteor. Soc., B-17 to B-24.

Cressman, G. P., 1959: An operational objective analysis system, Mon. Wea. Rev., 87, 367-374.

Gerrish, H. P., and H. W. Hiser, 1965: Meso-scale studies of instability patterns and winds in the tropics. Report 7, U. S. Army Electronics Labs., Fort Monmouth, N. J., 63 pp.

Hitschfeld, W., and J. Bordan, 1954: Errors inherent in the radar measurement of rainfall at attenuating wavelengths, J. Meteor., 2, 58-67.

Huff, F. A., 1967: The adjustment of radar estimates of storm mean rainfall with rain gage data, J. Appl. Meteor., 6, No. 1, 52-56.

Joss, J., J. C. Thams, and A. Waldvogel, 1968: The accuracy of daily rainfall measurements by radar. Proceedings 13th Conf. Radar Meteor., Montreal, Canada, Amer. Meteor. Soc., 448-451.

Maine, R., and D. J. Guantlett, 1968: Modifications to an operatioal numerical weather analysis system and application to rainfall, J. Appl. Meteor., 7, No. 1, 18-28.

Probert-Jones, J. R., 1962: The radar equation in meteorology. Quart. J. Roy. Met. Soc., 88, 485-495.

Shuman, F. G., 1957: Numerical methods in weather prediction: II Smoothing and filtering, Mon. Wea. Rev., 85, 357-361.

Wilk, K. E. and E. Kessler, 1970: Quantitative radar measurements of precipitation. Meteor. Monographs, 11, No. 33, 315-329.

Wilson, J. W., 1970a: Integration of radar and raingage data for improved rainfall measurement, J. Appl. Meteor., 9, No. 3, 489-497.

Wilson, J. W., 1970b: Operational measurement of rainfall with the WSR-57: state-of-art and recommendations. Final Report NSSL, NOAA Contract E22-80-70(N), The Center for the Environment and Man, Inc., Hartford, Conn.

Wilson, J. W., 1971: Use of rain gages to adjust radar estimates of rainfall. Final Report, NSSL, NOAA Contract E22-41-71(N), The Center for the Environment and Man, Inc., Hartford, Conn.

Woodley, W., and A. Herndon, 1970: A raingage evaluation of the Miami reflectivity-rainfall rate relation. J. Appl. Meteor., 9, No. 2, 258-263.

NATIONAL SEVERE STORMS LABORATORY

The NSSL Technical Memoranda, beginning with No. 28, continue the sequence established by the U. S. Weather Bureau National Severe Storms Project, Kansas City, Missouri. Numbers 1-22 were designated NSSP Reports. Numbers 23-27 were NSSL Reports, and 24-27 appeared as subseries of Weather Bureau Technical Notes. These reports are available from the National Technical Information Service, Operations Division, Springfield, Virginia 22151, for $3.00, and a microfiche version for $0.95. NTIS numbers are given below in parentheses.

No. 1 National Severe Storms Project Objectives and Basic Design. Staff, NSSP. March 1961. (PB-168207)

No. 2 The Development of Aircraft Investigations of Squall Lines from 1956-1960. B. B. Goddard. (PB-168208)

No. 3 Instability Lines and Their Environments as Shown by Aircraft Soundings and Quasi-Horizontal Traverses. D. T. Williams. February 1962. (PB-168209)

No. 4 On the Mechanics of the Tornado. J. R. Fulks. February 1962. (PB-168210)

No. 5 A Summary of Field Operations and Data Collection by the National Severe Storms Project in Spring 1961. J. T. Lee. March 1962. (PB-165095)

No. 6 Index to the NSSP Surface Network. T. Fujita. April 1962. (PB-168212)

No. 7 The Vertical Structure of Three Dry Lines as Revealed by Aircraft Traverses. E. L. McGuire. April 1962. (PB-168213)

No. 8 Radar Observations of a Tornado Thunderstorm in Vertical Section. Ralph J. Donaldson, Jr. April 1962. (PB-174859)

No. 9 Dynamics of Severe Convective Storms. Chester W. Newton. July 1962. (PB-163319)

No. 10 Some Measured Characteristics of Severe Storms Turbulence. Roy Steiner and Richard H. Rhyne. July 1962. (N62-16401)

No. 11 A Study of the Kinematic Properties of Certain Small-Scale Systems. D. T. Williams. October 1962. (PB-168216)

No. 12 Analysis of the Severe Weather Factor in Automatic Control of Air Route Traffic. W. Boynton Beckwith. December 1962. (PB-168217)

No. 13 500-Kc./Sec. Sferics Studies in Severe Storms. Douglas A. Kohl and John E. Miller. April 1963. (PB-168218)

No. 14 Field Operations of the National Severe Storms Project in Spring 1962. L. D. Sanders. May 1963. (PB-168219)

No. 15 Penetrations of Thunderstorms by an Aircraft Flying at Supersonic Speeds. G. P. Roys. Radar Photographs and Gust Loads in Three Storms of 1961 Rough Rider. Paul W. J. Schumacher. May 1963. (PB-168220)

No. 16 Analysis of Selected Aircraft Data from NSSP Operations, 1962. T. Fujita. May 1963. (PB-168221)

No. 17 Analysis of Methods for Small-Scale Surface Network Data. D. T. Williams. August 1963. (PB-168222)

No. 18 The Thunderstorm Wake of May 4, 1961. D. T. Williams. August 1963. (PB-168223)

No. 19 Measurements by Aircraft of Condensed Water in Great Plains Thunderstorms. George P. Roys and Edwin Kessler. July 1966. (PB-173048)

No. 20 Field Operations of the National Severe Storms Project in Spring 1963. J. T. Lee, L. D. Sanders and D. T. Williams. January 1964. (PB-168224)

No. 21 On the Motion and Predictability of Convective Systems as Related to the Upper Winds in a Case of Small Turning of Wind with Height. James C. Fankhauser. January 1964. (PB168225)

No. 22 Movement and Development Patterns of Convective Storms and Forecasting the Probability of Storm Passage at a Given Location. Chester W. Newton and James C. Fankhauser. January 1964. (PB-168226)

No. 23 Purposes and Programs of the National Severe Storms Laboratory, Norman, Oklahoma. Edwin Kessler. December 1964. (PB-166675)

No. 24 Papers on Weather Radar, Atmospheric Turbulence, Sferics, and Data Processing. August 1965. (AD-621586)

No. 25 A Comparison of Kinematically Computed Precipitation with Observed Convective Rainfall. James C. Fankhauser. September 1965. (PB-168445).

No. 26 Probing Air Motion by Doppler Analysis of Radar Clear Air Returns. Roger M. Lhermitte. May 1966. (PB-170636)

No. 27 Statistical Properties of Radar Echo Patterns and the Radar Echo Process. Larry Armijo. May 1966. The Role of the Kutta-Joukowski Force in Cloud Systems with Circulation. J. L. Goldman. May 1966. (PB-170756)

No. 28 Movement and Predictablity of Radar Echoes. James Warren Wilson. November 1966. (PB-173972)

No. 29 Notes on Thunderstorm Motions, Heights, and Circulations. T. W. Harrold, W. T. Roach, and Kenneth E. Wilk. November 1966. (AD-644899)

No. 30 Turbulence in Clear Air Near Thunderstorms. Anne Burns, Terence W. Harrold, Jack Burnham, and Clifford S. Spavins. December 1966. (PB-173992)

No. 31 Study of a Left-Moving Thunderstorm of 23 April 1964. George R. Hammond. April 1967. (PB-174681)

No. 32 Thunderstorm Circulations and Turbulence from Aircraft and Radar Data. James C. Fankhauser and J. T. Lee. April 1967. (PB-174860)

No. 33 On the Continuity of Water Substance. Edwin Kessler. April 1967. (PB-175840)

No. 34 Note on the Probing Balloon Motion by Doppler Radar. Roger M. Lhermitte. July 1967. (PB-175930)

No. 35 A Theory for the Determination of Wind and Precipitation Velocities with Doppler Radars. Larry Armijo. August 1967. (PB-176376)

No. 36 A Preliminary Evaluation of the F-100 Rough Rider Turbulence Measurement System. U. O. Lappe. October 1967. (PB-177037)

No. 37 Preliminary Quantitative Analysis of Airborne Weather Radar. Lester P. Merritt. December 1967. (PB-177188)

No. 38 On the Source of Thunderstorm Rotation. Stanley L. Barnes. March 1968. (PB-178990)

No. 39 Thunderstorm - Environment Interactions Revealed by Chaff Trajectories in the Mid-Troposphere. James C. Fankhauser. June 1968. (PB-179659)

No. 40 Objective Detection and Correction of Errors in Radiosonde Data. Rex L. Inman. June 1968. (PB-180284)

No. 41 Structure and Movement of the Severe Thunderstorms of 3 April 1964 as Revealed from Radar and Surface Mesonetwork Data Analysis. Jess Charba and Yoshikazu Sasaki. October 1968. (PB-183310)

No. 42 A Rainfall Rate Sensor. Brian E. Morgan. November 1968. (PB-183979)

No. 43 Detection and Presentation of Severe Thunderstorms by Airborne and Ground-Based Radars: A Comparative Study. Kenneth E. Wilk, John K. Carter, and J. T. Dooley. February 1969. (PB-183572)

No. 44 A Study of a Severe Local Storm of 16 April 1967. George Thomas Haglund. May 1969. (PB-184-970)

No. 45 On the Relationship Between Horizontal Moisture Convergence and Convective Cloud Formation. Horace R. Hudson. March 1970. (PB-191720)

No. 46 Severe Thunderstorm Radar Echo Motion and Related Weather Events Hazardous to Aviation Operations. Peter A. Barclay and Kenneth E. Wilk. June 1970. (PB-192498)

No. 47 Evaluation of Roughness Lengths at the NSSL-WKY Meteorological Tower. Leslie D. Sanders and Allen H. Weber. August 1970. (PB-194587)

No. 48 Behavior of Winds in the Lowest 1500 ft in Central Oklahoma: June 1966 - May 1967. Kenneth C. Crawford and Horace R. Hudson. August 1970.

No. 49 Tornado Incidence Maps. Arnold Court. August 1970. (COM-71-00019)

No. 50 The Meteorologically Instrumented WKY-TV Tower Facility. John K. Carter. September 1970. (COM-71-00108)

No. 51 Papers on Operational Objective Analysis Schemes at the National Severe Storms Forecast Center. Rex L. Inman. November 1970. (COM-71-00136)

No. 52 The Exploration of Certain Features of Tornado Dynamics Using a Laboratory Model. Neil B. Ward. November 1970. (COM-71-00139)

No. 53 Rawinsonde Observation and Processing Techniques at the National Severe Storms Laboratory. Stanley L. Barnes, James H. Henderson and Robert J. Ketchum. April 1971.

No. 54 Model of Precipitation and Vertical Air Currents. Edwin Kessler and William C. Bumgarner. June 1971.

No. 55 The NSSL Surface Network and Observations of Hazardous Wind Gusts. Operations Staff. June 1971.

No. 56 Pilot Chaff Project at the National Severe Storms Laboratory. Edward A. Jessup. November 1971.

No. 57 Numerical Simulation of Convective Vortices. Robert P. Davies-Jones and Glenn T. Vickers. November 1971.

No. 58 The Thermal Structure of the Lowest Half Kilometer in Central Oklahoma: December 9, 1966 - May 31, 1967. R. Craig Goff and Horace R. Hudson. July 1972.

No. 59 Cloud-to-Ground Lightning Versus Radar Reflectivity in Oklahoma Thunderstorms. Gilbert D. Kinzer. September 1972.

No. 60 Simulated Real Time Displays of Velocity Fields by Doppler Radar. L. D. Hennington and G. B. Walker. November 1972.

No. 61 Gravity Current Model Applied to Analysis of Squall-Line Gust Front. Jess Charba. November 1972.

No. 62 Mesoscale Objective Map Analysis Using Weighted Time-Series Observations. Stanley L. Barnes. March 1973.

No. 63 Observations of Severe Storms on 26 and 28 April 1971. Charles L. Vicek. April 1973.

No. 64 Meteorological Radar Signal Intensity Estimation. Dale Simmans and R. J. Doviak. September 1973.

No. 65 Radiosonde Altitude Measurement Using Double Radiotheodolite Techniques. Stephan P. Nelson. September 1973.

No. 66 The Motion and Morphology of the Dryline. Joseph T. Schaefer. September 1973.

☆GPO 1974 — 784-575/1255 REGION NO. 8